



ORIGINAL RESEARCH ARTICLE

Friction Stir Back Extrusion of Cu-5 vol.% Ti₂SnC Composite

Amirhossein Jahani, Hamed Jamshidi Aval, Mohammad Rajabi, and Roohollah Jamaati

Submitted: 16 February 2023 / Revised: 13 July 2023 / Accepted: 23 July 2023

The current study investigated the effects of the wire diameter on the microstructure, mechanical, electrical, and wear properties of the friction stir back extruded copper matrix composite reinforced by 5 vol.% Ti₂SnC. In this regard, friction stir back extrusion was performed using a rotational speed of 600 rpm and an extrusion speed of 25 mm/min. According to the results, composite wire with a diameter of 3 mm had a finer grain size than composite wire with a diameter of 5 mm. Also, composite wire with a diameter of 5 mm demonstrated desirable interfacial bonding and more homogenous distribution. Due to the higher temperature and plastic deformation during FSBE, a greater amount of Cu (Sn) solid solution and Cu₈₁Sn₂₂ intermetallic was generated in the microstructure by increasing the composite wire diameter. Furthermore, increasing the composite wire diameter from 3 to 5 mm improved the ultimate tensile strength, hardness, wear resistance, and electrical conductivity by 13, 10, 53, and 5%, respectively. The electrical conductivity of the composite wire with diameters of 3 and 5 mm was 84.65 ± 1.76 and 89.21 ± 1.43 IACS, respectively. Finally, Cu-5 vol.% Ti₂SnC composite wire with a diameter of 5 mm showed 7% lower electrical conductivity and 85% higher wear resistance than FSBE-processed pure copper wire with a similar diameter.

Keywords Cu-5 vol.% Ti₂SnC composite wire, electrical conductivity, friction stir back extrusion, wire diameter

1. Introduction

The high thermal and electrical conductivity of pure copper has led to its widespread use in a wide range of industries, particularly the electrical industry (Ref 1). The durability of materials used in most engineering fields depends on their surface properties, but pure copper has a low hardness and wear resistance. Copper reinforcement is a method for preventing the premature failure of samples due to low strength and wear resistance. Considering the rapid progress in industries and advanced technologies, such as the development of advanced materials that boast excellent strength, thermal, and electrical conductivity, it is imperative to select a new phase material for improving the properties of the copper matrix. An example of copper-based equipment is electrical switching contacts, in which high mechanical stability and good electrical conductivity are desirable. In this regard, it is possible to benefit from combining the excellent properties of ceramics and metals (Ref 2, 3).

A new material called MAX phase possesses some characteristics of metals, such as electrical conductivity, thermal conductivity, and machinability, and some characteristics of

ceramics, such as high elastic moduli and high-temperature strength. In the MAX phase, M represents a transition metal, A represents an element of the periodic table from groups 13 to 16, and X stands for carbon or nitrogen. Among more than 155 MAX-phase materials, Ti₂SnC has the highest electrical conductivity, good machinability, strength, and a low friction coefficient, making it an effective reinforcement for copper matrix composites (Ref 4).

There are two general methods for fabricating copper matrix composites (CMCs), namely the liquid and solid states (Ref 5). In the liquid state method, the reinforcing material is added to the copper matrix in liquid form, either as a powder or as a liquid suspension. In the solid state method, the reinforcing material is added to the matrix in a solid form, such as a fiber or a thin sheet. Both methods have their advantages and disadvantages. Among the most important challenges associated with liquid state methods are wettability, the formation of reaction layers, and porosity (Ref 6). In this regard, friction stir back extrusion (FSBE) is a new thermomechanical technique based on friction stir processing, which is proper for fabricating composite materials. This process has been recently used for fine-grained wires and tube fabrication.

The fabrication of metal wires has been reported in several studies. Ma et al. (Ref 7) manufactured copper wires strengthened by oxide dispersion from the initial powder material with the FSBE process in one step. The results showed that the average grain size was 40 times smaller than the primary material due to the large shear deformation. Furthermore, the mechanical properties were higher or comparable to conventional strengthened copper materials sintered and then extruded with oxide dispersion. Akbari and Asadi (Ref 8) optimized the rotational speed, extrusion speed, and wire diameter parameters in the FSBE process for brass wire. This optimization was considered by grain size, microhardness, and ultimate tensile

Amirhossein Jahani, Hamed Jamshidi Aval, Mohammad Rajabi, and Roohollah Jamaati, Department of Materials Engineering, Babol Noshirvani University of Technology, Shariati Avenue, Babol 47148-71167, Iran. Contact e-mail: h.jamshidi@nit.ac.ir.

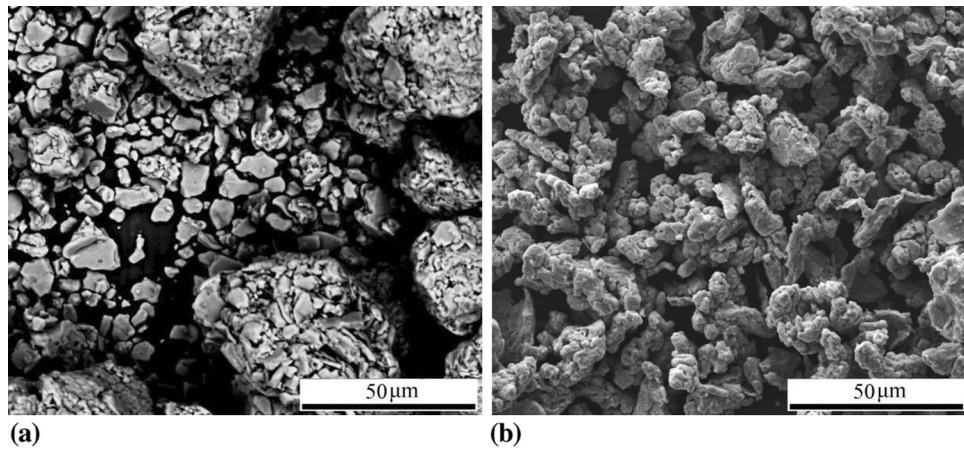


Fig. 1 SEM image of; (a) Ti_2SnC powder, and (b) copper powder

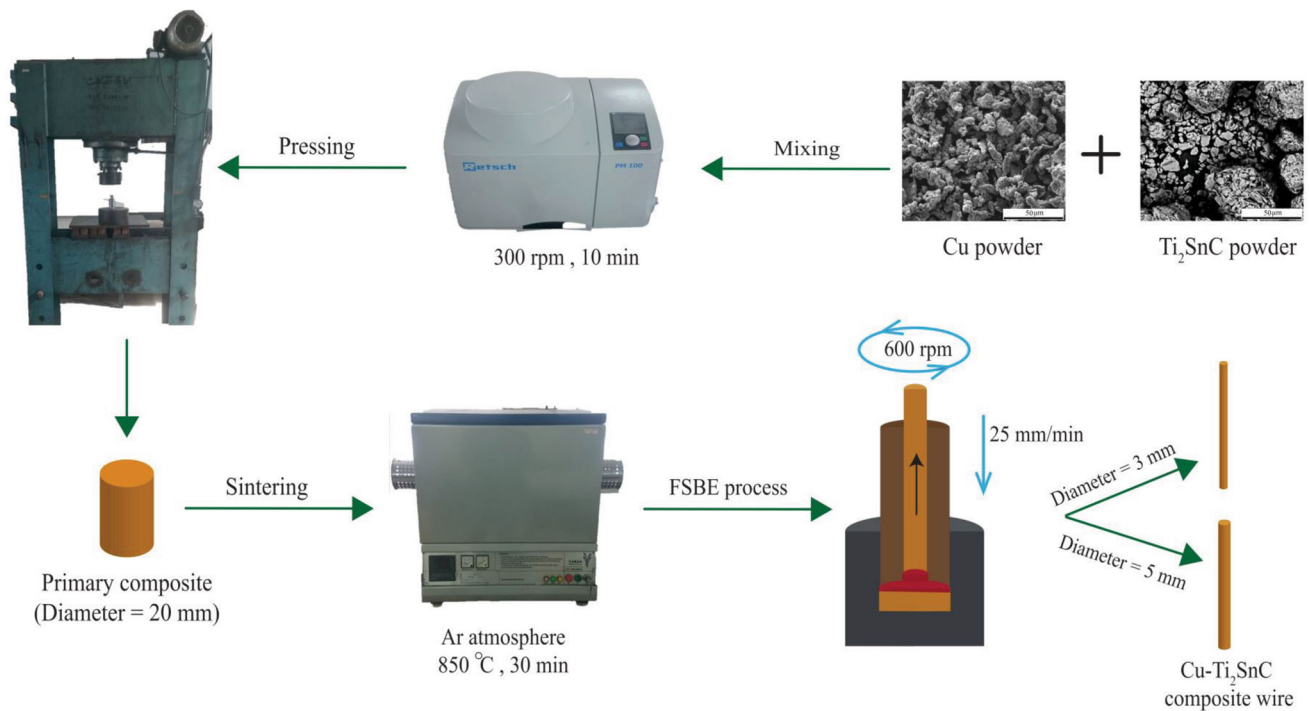


Fig. 2 A schematic view of $\text{Cu-Ti}_2\text{SnC}$ composite wire fabrication using FSBE process

strength of the fabricated wires. They reported that the optimum rotational speed, extrusion speed, and wire diameter were 500 rpm, 31.5 mm/min, and 6 mm, respectively. Similarly, Ansari et al. (Ref 9) optimized the same FSBE process parameters for pure Mg with the Taguchi method. The optimum wire diameter was 5 mm because of the finest grain size.

Baffari et al. (Ref 10) used the FSBE process to produce three magnesium alloy wires with 5, 7, and 9 mm diameters. The numerical results indicated that helical material flow occurred in the die channel, and a large hole of 9 mm diameter was observed in the center of the wire. Reducing the extrusion ratio (i.e., the ratio of wire diameter to primary sample diameter) increased the mechanical strength due to higher compaction levels or a higher pressure in the chamber. In another study, using the FSBE process, Baffari et al. (Ref 11)

produced an aluminum matrix composite from its chips reinforced with powder particles. Defect-free wires with a diameter of 3 mm were fabricated. Also, numerical simulations suggested that helical material flow occurred during the FSBE process.

Numerous researchers have conducted extensive research on the fabrication of metal wires using the FSBE process. However, the effects of extrusion ratio on microstructure, mechanical properties, electrical conductivity, and wear resistance of FSBE-processed copper matrix composite reinforced with Ti_2SnC reinforcement have yet to be investigated. The extrusion ratio has a significant impact on the microstructure and properties of the extruded wire due to its influence on plastic deformation and wire exit velocity. This study employed FSBE to generate copper matrix composite wires with 3 and 5

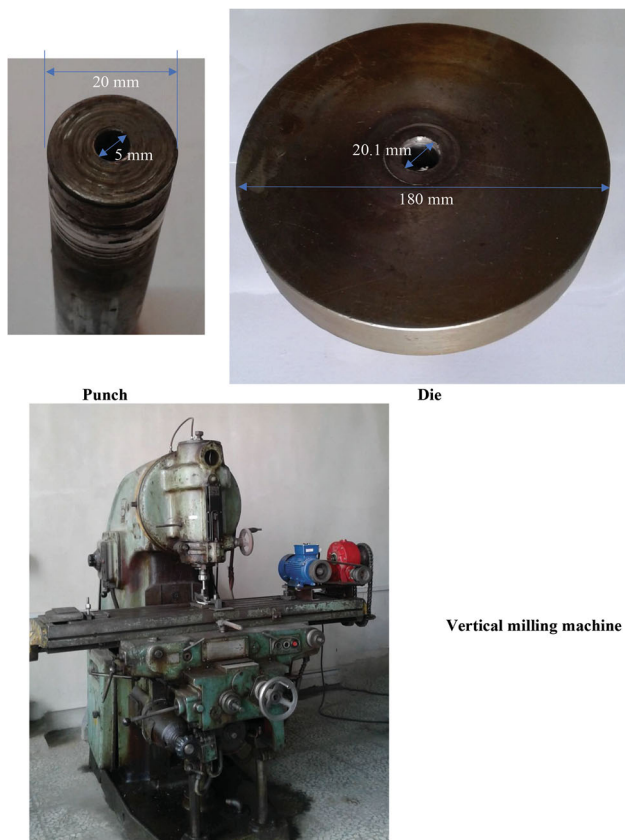


Fig. 3 The die, punch, and vertical milling machine used for FSBE process

mm diameters and a constant Ti_2SnC content of 5 vol. As a first step to fabricate the composite wires, Cu- Ti_2SnC composites were made using powder metallurgy. Afterward, the microstructure, mechanical properties, electrical conductivity, and tribological properties of the composite wire fabricated with a rotational speed of 600 rpm and an extrusion speed of 25 mm/min were investigated.

2. Experimental Procedure

This study included two primary powders, Cu as the matrix and Ti_2SnC as the reinforcement. The powders had particle sizes of 10-40 μm and 0.5-20 μm , respectively, and purity requirements of 99%. In Fig. 1, scanning electron microscope (SEM) images of the materials are shown. Cu with 5 vol. % Ti_2SnC was mixed in a Planetary Ball Mill PM 100 to prepare composite wires with two diameters of 3 and 5 mm. Ar gas was poured into the container before putting the container in the PM 100 device. The powder set was mixed with steel balls with a diameter of 10 mm for 10 minutes at 300 rpm. In order to press the material and produce a primary composite with a diameter of 20 mm and length of 30 mm, the mixed powder was poured into the CK45 die steel at a pressure of 150 bar, and then a cylindrical primary composite was placed in a furnace with protective Ar gas at 850 °C for 30 min.

The sintered primary composite was put into the FSBE process chamber with outer diameter, inner diameter, and height of 50, 20, and 70 mm, respectively. A punch with an

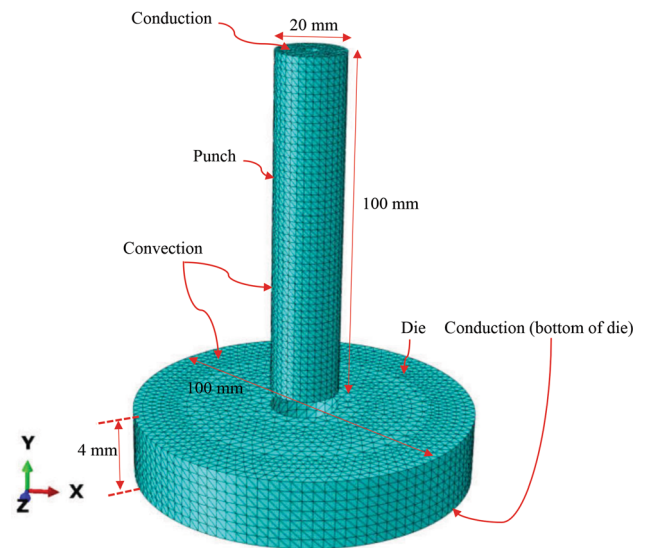


Fig. 4 The boundary condition and geometric model used in the simulation of FSBE process

Table 1 Johnson–Cook parameters used in the simulation of FSBE process

Constant	A	B	<i>n</i>	C	<i>m</i>
Value	90, MPa	292, MPa	0.31	0.029	0.98

outer diameter of 20 mm, a height of 70 mm, and two different hole sizes of 3 and 5 mm were then used for FSBE. According to previous studies (Ref 12, 13), optimization techniques can be used to determine optimal parameters for the FSBE process. Nonetheless, based on preliminary experiments and previous research (Ref 14), the FSBE process in this study was performed at a rotational speed of 600 rpm and an extrusion speed of 25 mm/min. The composite wires with 3- and 5-mm diameters were named CW-3 and CW-5, respectively, and the pure copper wire with 5 mm diameter was named PW-5. A schematic of the produced wires and all the mentioned processes is shown in Fig. 2. Also, Fig. 3 illustrates the die, punch, and vertical milling machine used in the FSBE process.

After extrusion, different samples were prepared to check the microstructure, mechanical properties, wear resistance, and electrical conductivity. In order to investigate its microstructure, the composite wire cross section was prepared using SiC sandpaper and alumina suspension. After this, the cross section of the samples was etched with a reagent consisting of 85 ml distilled water, 15 ml HCl, and 5 g $FeCl_3$ to reveal their microstructure. The microstructure was examined using the NGF-120A optical microscope and a Philips-XL30FSEM scanning electron microscope (SEM) equipped with an EDS detector. In addition, a Rigaku Ultima IV x-ray diffraction machine was used for phase analysis. The hardness of the samples was measured using a KOOPA Universal (UV1) microhardness tester with a force of 100 gr and a duration time of 15 s. The tensile test was performed according to the ASTM E8 standard using a crosshead speed of 1 mm/min. The

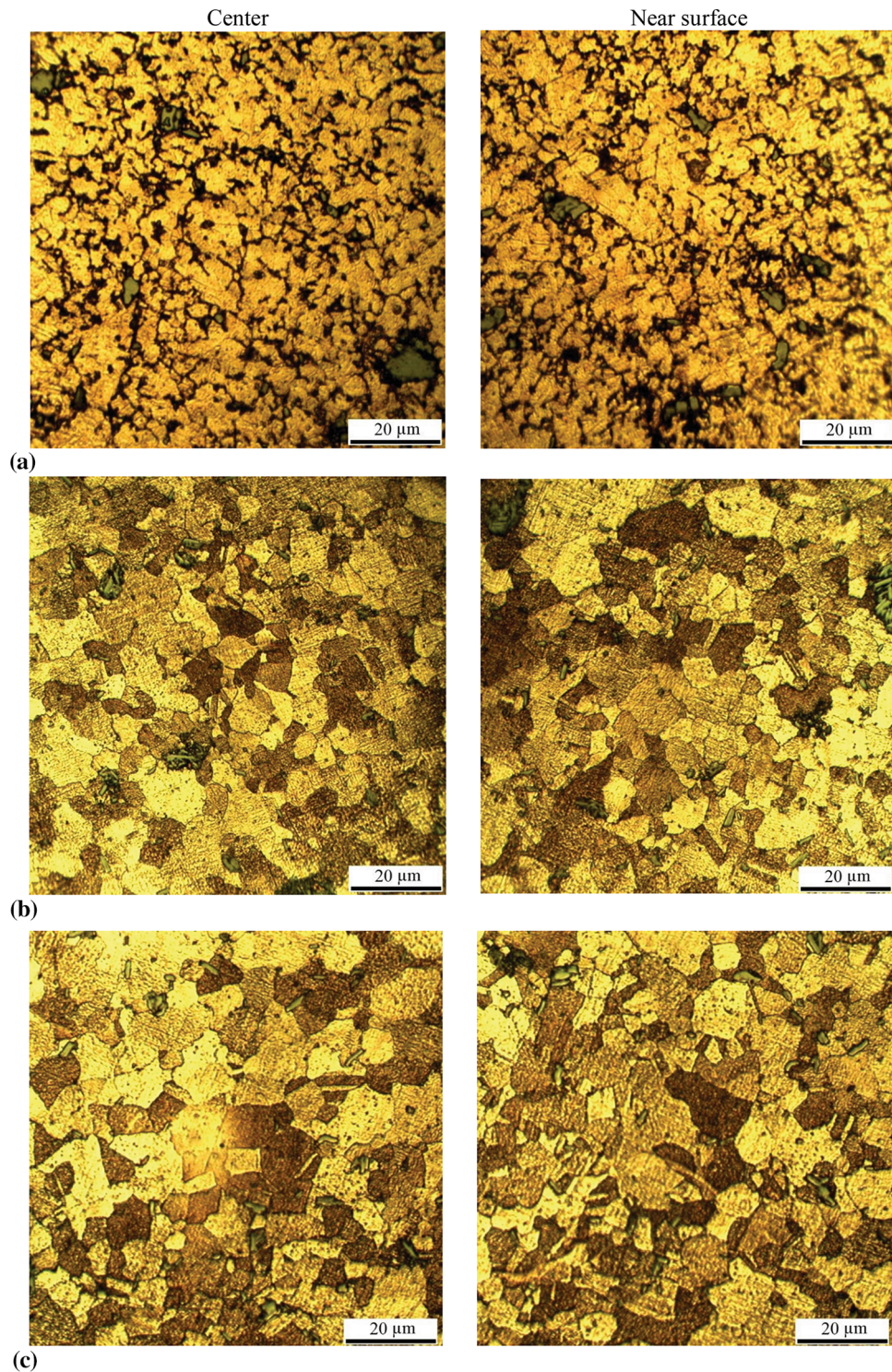


Fig. 5 Optical microscopy image of microstructure of; (a) composite sample before FSBE, (b) sample CW-3, (c) sample CW-5, (d) sample PW-5

electrical conductivity test was conducted on different samples using the ASTM F1711 standard. The wear test was performed according to the ASTM G99 standard using the pin-on-disc method. The counterface was made of steel with a hardness of 60 HRC. The wear test was carried out under a load of 20 N at a distance of 2000 m. After the tensile and wear test, the fracture and wear surfaces of the samples were examined by SEM.

3. Friction Stir Back Extrusion Simulation

Based on the method described in the previous study (Ref 15), the finite element method was employed to simulate the FSBE process and estimate changes in plastic strain and temperature. The punch and die in this model are considered rigid bodies, and the copper matrix composite is considered a plastic material. As shown in Fig. 4, the dimensions of the

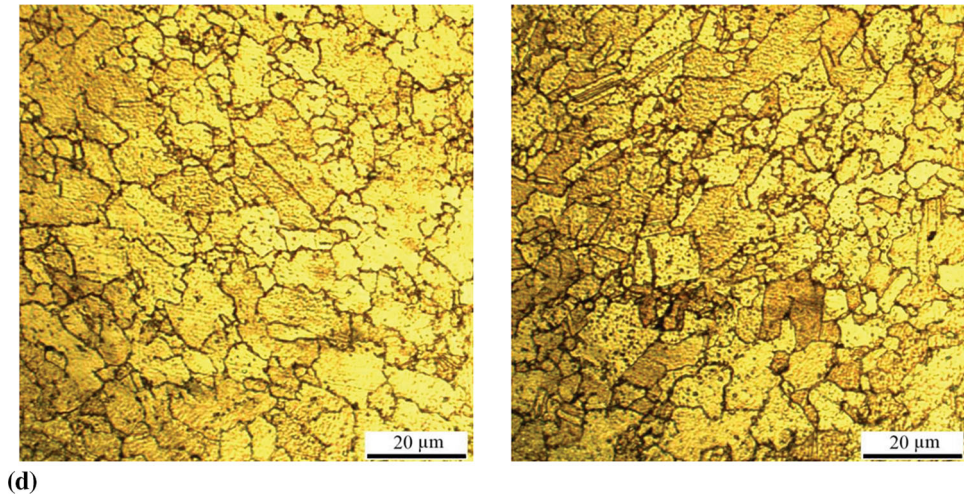


Fig. 5 continued

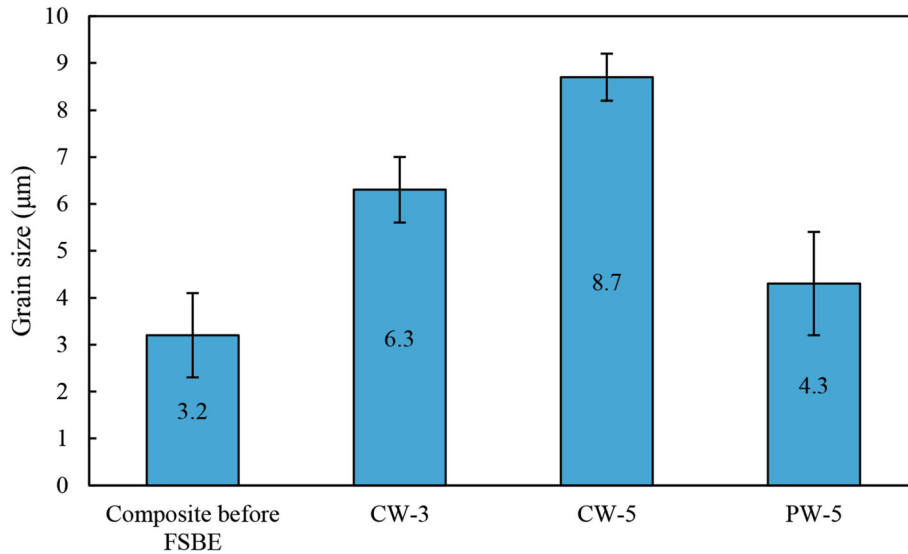


Fig. 6 The grain size distribution of different samples

punch and die corresponded to those used in the experimental work. In the simulation, the die was fixed from the bottom surface, and the vertical and rotational speed of the punch was taken into account. The conduction mechanism and coefficient of $1000 \text{ W/m}^2 \text{ }^\circ\text{C}$ were considered for the punch contact surface with the FSBE machine and the bottom surface of the die. On other surfaces, heat transfer was considered a convection mechanism with a coefficient of $20 \text{ W/m}^2 \text{ }^\circ\text{C}$. Also, the heat transfer between the copper matrix composite and the die and punch contact surfaces was considered to be a conduction mechanism with a coefficient of $10000 \text{ W/m}^2 \text{ }^\circ\text{C}$.

A general contact interaction was used to account for all contact sites between the workpiece and the punch. The Coulomb friction model was employed to represent the friction between the punch and the workpiece. Temperature, strain rate, and strain are all factors that influence the material flow stress

in the process. Therefore, the Johnson–Cook model was utilized to model the flow of copper matrix material as follows:

$$\sigma = [A + B\varepsilon^n] \left[1 + C \ln \left(\frac{\dot{\varepsilon}}{\dot{\varepsilon}_0} \right) \right] \left[1 - \left(\frac{T - T_r}{T_m - T_r} \right)^m \right] \quad (\text{Eq 1})$$

where ε is the equivalent plastic strain, $\dot{\varepsilon}$ is the equivalent plastic strain rate, T is the instantaneous temperature of the process, and A , B , n , m , $\dot{\varepsilon}_0$, and C are the material parameters. T_r and T_m are reference and melting point temperatures, respectively. The parameters related to the material's properties are reported in Table 1. The C3D8T (an 8-node thermally coupled brick, trilinear displacement, and temperature) elements were used for composite wire simulation. The FSBE was modeled using ABAQUS software in Arbitrary Lagrangian–Eulerian (ALE) mode. The number of elements considered in the initial

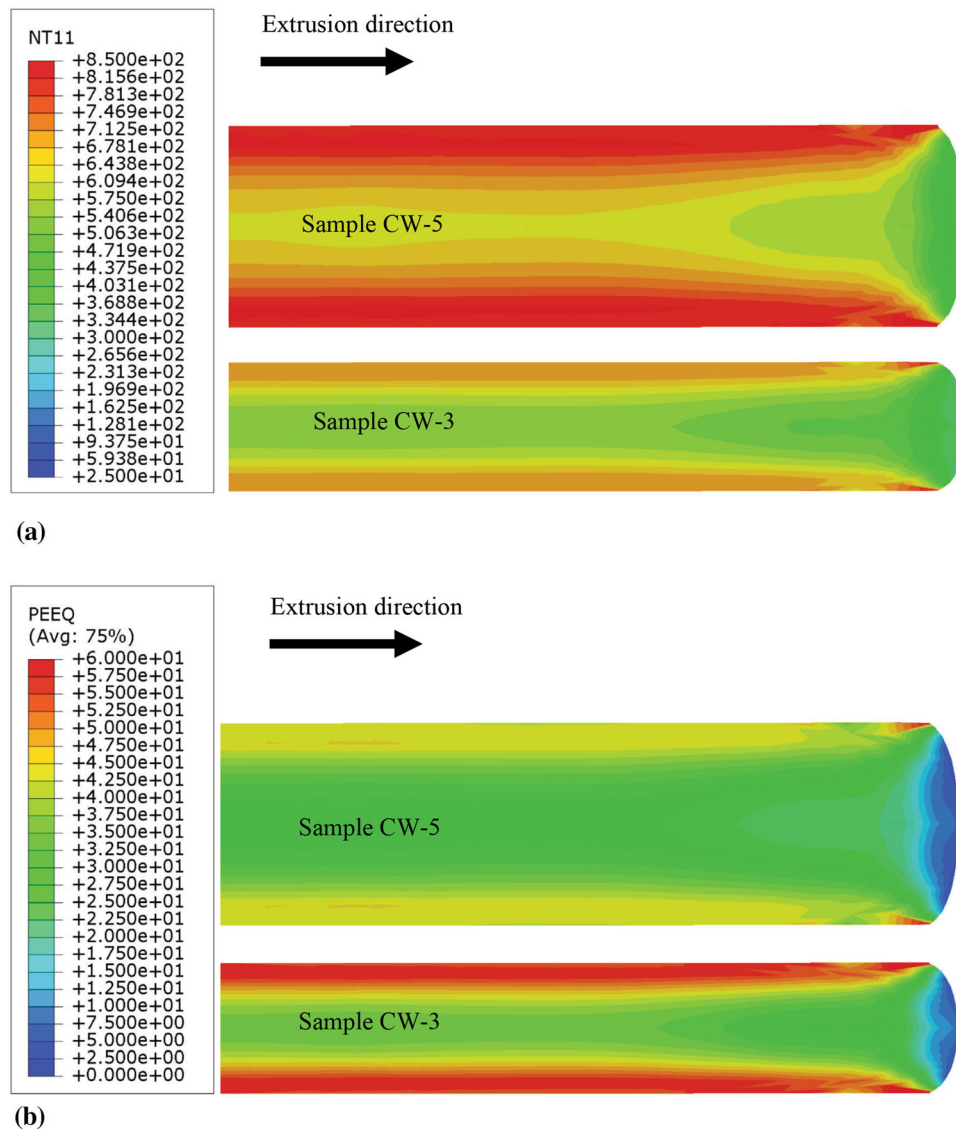


Fig. 7 The predicted temperature and plastic strain in different samples; (a) temperature profile, and (b) plastic strain profile

composite, punch, and die was 245356, 436780, and 1298452, respectively.

4. Results and Discussion

The heat induced by friction between the die surface and the material during the FSBE process resulted in a higher temperature than the processed material's recrystallization temperature. This high temperature and plastic deformation led to dynamic recrystallization (DRX), the most dominant mechanism of microstructure change during friction stir processes (Ref 16). Figure 5 shows optical microscope images of the cross section of the different samples. Also, Fig. 6 displays the average grain size of different samples. Figure 3(a) illustrates the primary composite sample with an average grain size of $3.2 \mu\text{m}$. The presence of Ti_2SnC , as an obstacle to grain growth, prevented grains from becoming coarse, and no

difference was observed between the center and the surface of the wire.

Figure 5(b), (c), and (d) shows the microstructure of extruded wires of CW-3, CW-5, and PW-5. The average grain size of the CW-3, CW-5, and PW-5 samples is $6.3 \mu\text{m}$, $8.7 \mu\text{m}$, and $4.3 \mu\text{m}$, respectively. Clearly, the average grain size of the extruded wires is higher than the primary composite. Two main factors determine the grain size of samples in the FSBE process: temperature and plastic strain (Ref 17). With increasing temperature or decreasing plastic strain, grain size increases. A three-dimensional thermomechanical model was used to predict thermomechanical evolution during FSBE to investigate the influence of temperature on grain size. It is worth mentioning that the model was verified using experimental temperature measurement results. Figure 7 and Table 2 indicate that in the extrusion of wire with a diameter of 3 mm, a lower temperature and greater plastic strain were created than in the extrusion of wire with a diameter of 5 mm. Furthermore, it is important to note that the difference in temperature and

plastic strain between the surface and center of the wire is significant. When the wire diameter was increased from 3 to 5 mm, the predicted cooling rate decreased from 0.8 to 0.5 °C/s, resulting in grain growth. The correlation between grain size reduction and wire diameter reduction demonstrated a dominant influence of temperature and plastic strain on grain size reduction.

PW-5 has a smaller grain size than CW-3 and CW-5 due to the absence of Ti₂SnC and the higher cooling rate. The lack of reinforcement particles increased plastic strain, followed by an increase in nucleation sites. On the other hand, since the PW-5 sample lacks the MAX phase, its thermal conductivity is greater than that of the CW-3 and CW-5 samples, resulting in a greater cooling rate. Accordingly, compared to sample CW-5, finer

Table 2 The maximum temperature and plastic strain rate of different samples

Sample label	Temperature, °C	Plastic strain, mm/mm
CW-3	820	59.4
CW-5	843	51.8
PW-5	829	52.3

grain size can be formed in sample PW-5 due to the higher plastic strain and lower temperature (as reported in Table 2).

The phase analysis of the primary composite and the extruded wires is shown in Figure 8. The dominant phases in the primary composite were Cu and Ti₂SnC. On the other hand, in addition to these phases, the samples CW-3 and PW-5 also included the Cu₈₁Sn₂₂ phase, indicating that this phase was either not formed in the main composite sample or lower than the XRD detection limit. Moreover, the presence of this new phase suggests an interface reaction between matrix and reinforcement during FSBE under the influence of plastic deformation and heat. Figure 9 shows the texture parameters of different samples. Besides, the texture parameter was used to calculate grain orientation, expressed according to the following equation (Ref 18):

$$TP_{hkl} = \frac{I_{hkl}/R_{hkl}}{\frac{1}{n} \sum_0^n (I_{hkl}/R_{hkl})} \quad (\text{Eq 2})$$

where I_{hkl} is the intensity of $\{hkl\}$ in the primary composite samples, and extruded wires, and R_{hkl} is the intensity of $\{hkl\}$ in the same sample with random orientation for n peaks. The texture parameter greater than 1 indicates the preferred orientation of that plane. The highest texture parameter of the primary composite, with a value of 1.13, was found in the (111) plane. With the FSBE process applied to the primary compos-

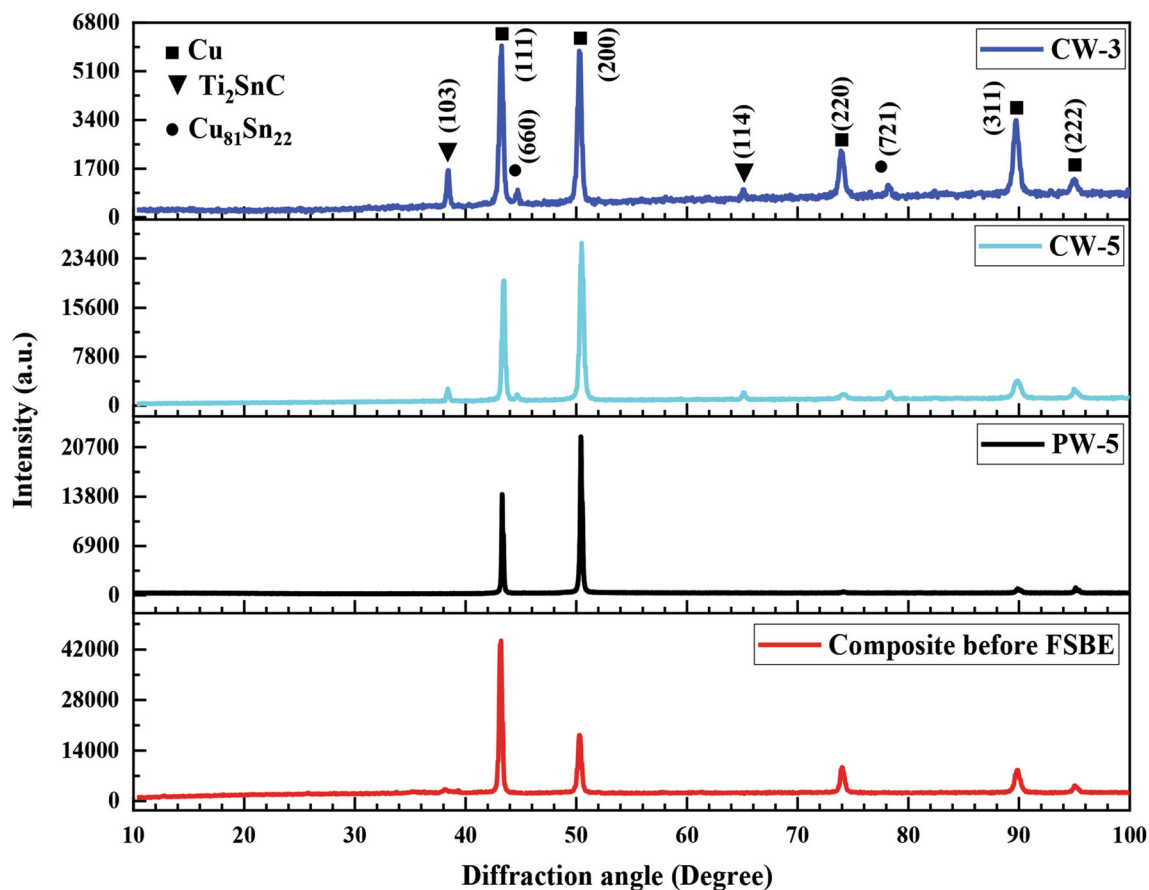


Fig. 8 X-ray diffraction pattern of different samples

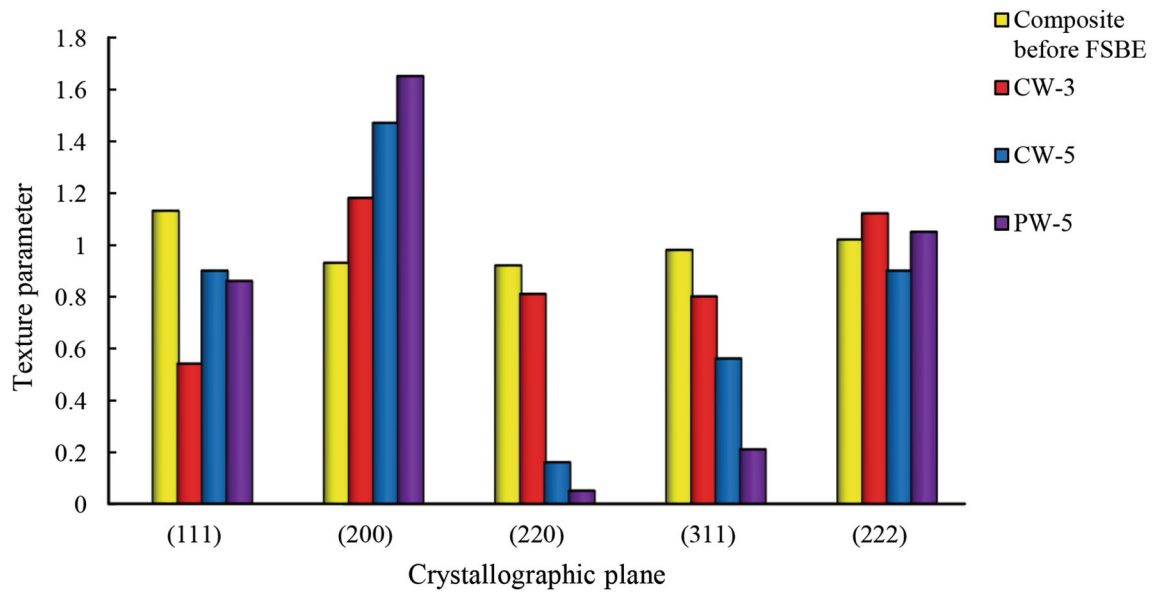


Fig. 9 The texture parameters of different samples

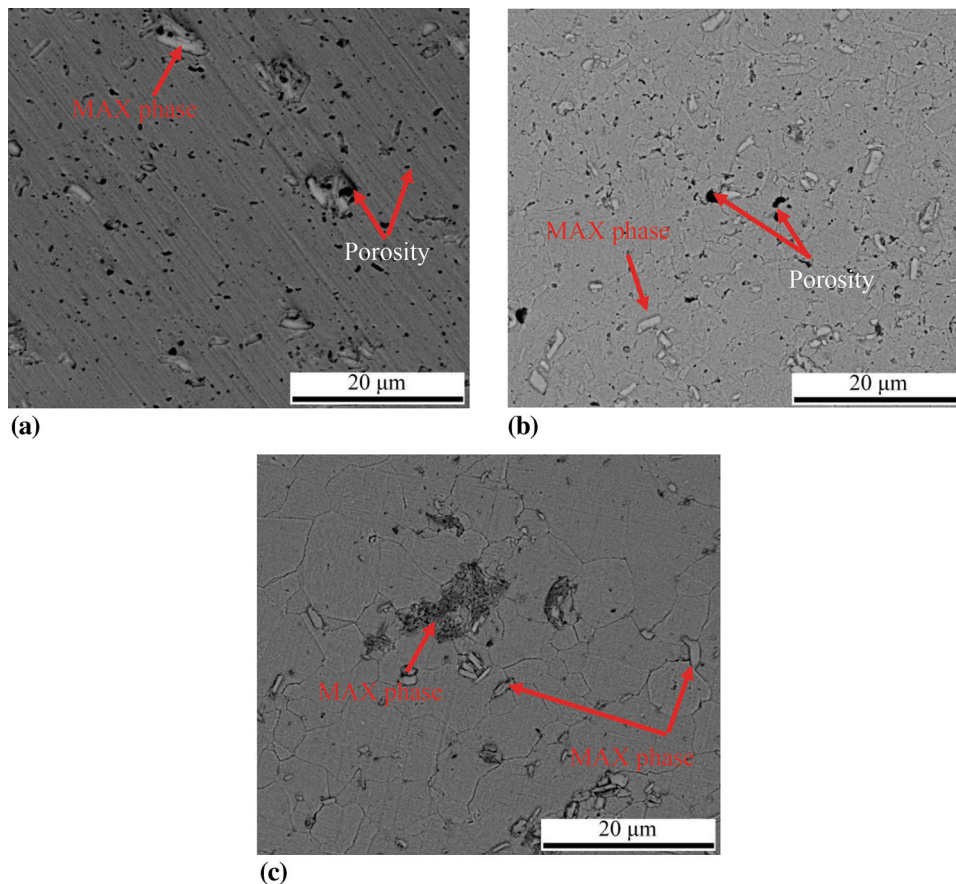
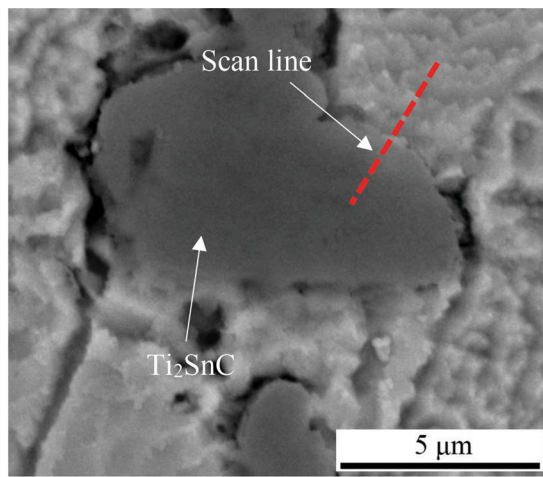


Fig. 10 SEM micrograph of; (a) Cu-Ti₂SnC composite before FSBE, (b) sample CW-3, (c) sample CW-5

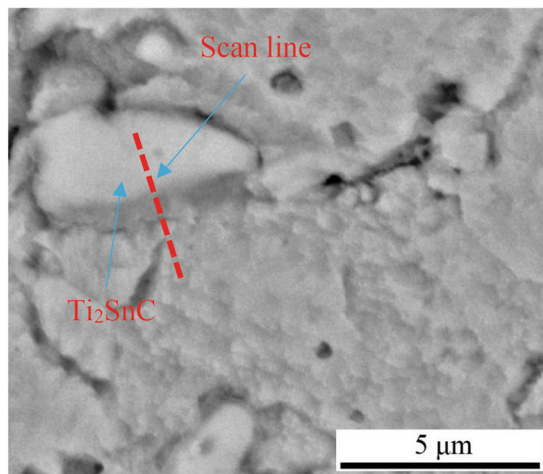
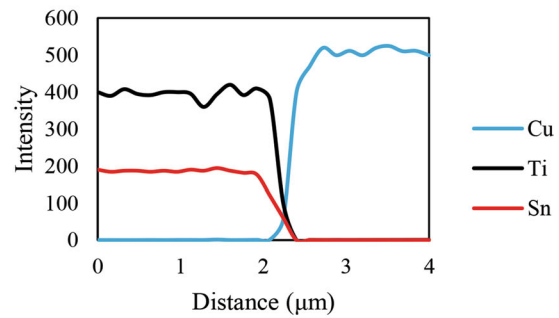
ite, the crystallographic plane with the highest texture parameter of the extruded wires changed. However, it should be noted that a strong crystallographic texture cannot be formed after FSBE. In this situation, the effect of the crystallographic texture

on the properties (e.g., mechanical properties) of the FSBE-processed wire can be omitted.

Figure 10 depicts SEM images of the matrix interface and the reinforcement interface of the primary composite samples



(a)



(b)

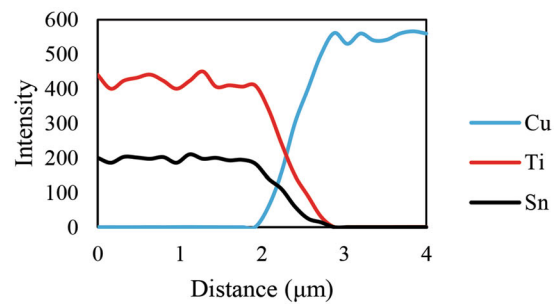


Fig. 11 The SEM image of the interface between the reinforcement and matrix of; (a) sample CW-3, (b) sample CW-5

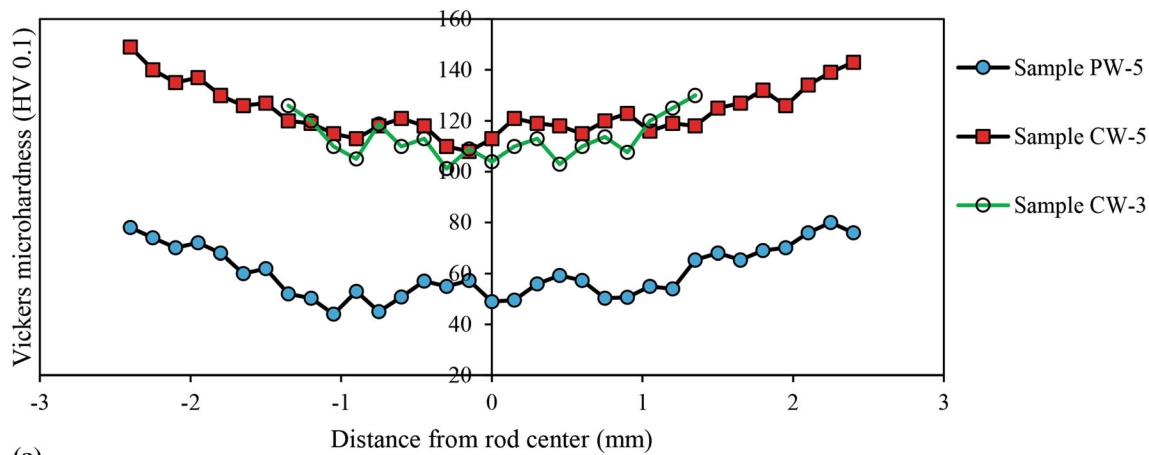
CW-5 and CW-3. While a desirable interfacial bonding reduces the porosity content, an undesirable interfacial bonding destroys the physical and mechanical properties of the copper matrix composite (Ref 19, 20). The primary composite contained a large amount of porosities. However, performing the FSBE process effectively removed a high percentage of them. In sample CW-5, the material flow was facilitated by the higher temperature and plastic strain during the FSBE (as predicted by simulation). In this condition, the matrix material readily captured Ti_2SnC particles, whereas the matrix material of sample CW-3 did not move as easily as sample CW-5. Overall, as shown in Fig. 10(b) and (c), sample CW-5 had lower porosities or better interface bonding than sample CW-3.

Figure 11 shows the line scan analysis at the reinforcement and copper matrix interface of different samples. As can be seen, interdiffusion between Cu and Sn occurred at the interface. According to EDS analysis and XRD results, the layer formed at the interface can be a solid solution of Cu (Sn) or $Cu_{81}Sn_{22}$ phase. Moreover, high temperature and plastic strain during FSBE provided the proper conditions for the reaction of the alloying elements and the formation of intermetallic phases. Unlike the primary composite, the composite wires had lower porosities and a more continuous interface, facilitating intermetallic phase formation. Interdiffusion between Cu and Sn resulted in stronger bonding between

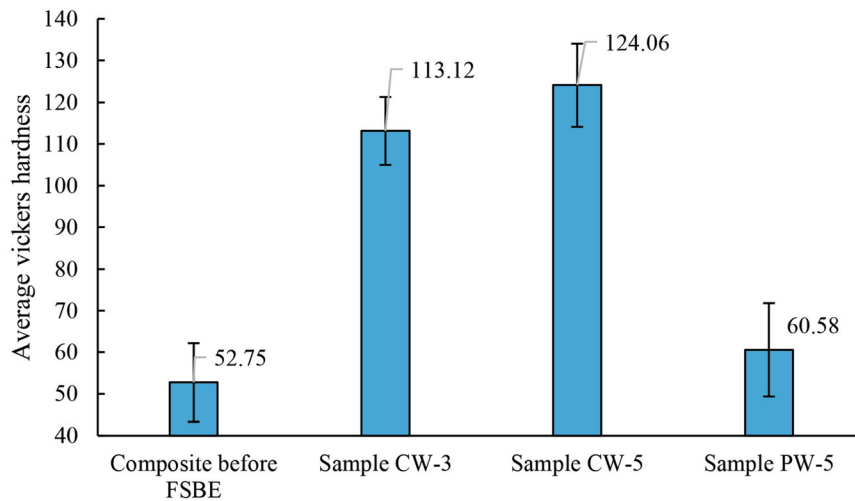
Cu and Ti_2SnC in the composite. Also, the sample CW-5 exhibited greater interdiffusion than the sample CW-3 due to its higher temperature and plastic strain.

The microhardness profile of the different samples is shown in Fig. 12. According to the microhardness profile, the microhardness of the primary composite is lower than that of the FSBE-processed composite samples. Following the FSBE process, the hardness of the wire at its surface was greater than at its center. These two areas did not exhibit significant changes in grain size, and the distribution of the MAX phase was similar in these areas. However, during the extrusion process, the plastic strain in the wire edge regions was greater than in the central regions (Ref 21-23). Moreover, the increase in dislocation density and residual stress in the edge regions of a wire can effectively increase its hardness compared to its central regions.

The average microhardness of the primary composite of samples PW-5, CW-3, and CW-5 was 52.75, 60.58, 113.12, and 124.06 HV, respectively. Interestingly, the microhardness of extruded wires, even pure copper wire, was higher than the primary composite. This increase in microhardness can be attributed to the plastic strain induced during the FSBE process, decreasing porosity, and solid solution formation during FSBE. Furthermore, compared with pure copper wire, the composite



(a)



(b)

Fig. 12 (a) Vickers microhardness profile and (b) average hardness of different samples

wires with Ti_2SnC reinforcement particles exhibited a further increase in hardness.

Figure 13 shows the stress–strain curve and tensile test properties of extruded wires. The ultimate tensile strength of samples PW-5, CW-3, and CW-5 was 216.91, 384.09, and 432.13 MPa, respectively. Changes in yield and ultimate tensile strength were similar to changes in hardness, and the elongation of samples increased as hardness decreased. Moreover, the yield strength and ultimate tensile strength increased significantly with the increase in composite wire diameter. Several strengthening mechanisms can be considered in the Cu- Ti_2SnC composite, including grain refinement, Orowan strengthening, solid solution strengthening, dislocation density resulting from the difference in coefficients of thermal expansion (CTE), and elastic modulus and load transfer mechanisms (Ref 24-27).

Observations revealed a grain refinement increment at the grain boundary, which resisted dislocation movement again. Similarly, the fine and hard particles resisted dislocation movement during Orowan strengthening, particularly at grain boundaries. As seen in Fig. 5, The grain size of sample CW-3 was smaller than that of sample CW-5; however, the low porosity and good interface between reinforcement and copper matrix resulted in higher strength and hardness in sample CW-5. The XRD and EDS results indicate that Cu (Sn) solid solution and $\text{Cu}_{81}\text{Sn}_{22}$ phase were formed in the composite wires. Therefore, this mechanism can be considered for

strengthening composite wires. Due to higher temperature and greater plastic strain in sample CW-5, more $\text{Cu}_{81}\text{Sn}_{22}$ phase was formed. Thus, the strength increment generated by this mechanism was greater in sample CW-5 than in sample CW-3.

The difference in coefficients of thermal expansion (CTE) of copper ($17.2 \times 10^{-6} \text{ k}^{-1}$) and Ti_2SnC ($10 \times 10^{-6} \text{ k}^{-1}$) and the elastic modulus of copper (89 GPa) and Ti_2SnC (228 GPa) caused internal stresses, which led to the formation of dislocations. In this mechanism, the interaction between these dislocations boosted the strength. It should be noted that finer particles enhanced strengthening through this mechanism. Since finer particles were formed in sample CW-5 than in sample CW-3 due to the higher plastic strain, more dislocations were obtained based on the difference between the CTE and elastic modulus. Finally, this mechanism resulted in a greater strength increment in sample CW-5. The highest elongation value of 77.32 % was observed for sample PW-5. Increasing the Ti_2SnC phase reduced the elongation of composite wires because the movement of dislocations was restricted by Ti_2SnC particles (Ref 28). Due to lower porosities and a better interface between reinforcement and copper matrix, sample CW-5, with a value of 38.15%, had a higher elongation than sample CW-3, with a value of 34.25%.

Figure 14(a), (b), and (c) shows SEM images of fracture surfaces of samples CW-5, CW-3, and PW-5. It is evident that all extruded wires have dimples on their fracture surface. This

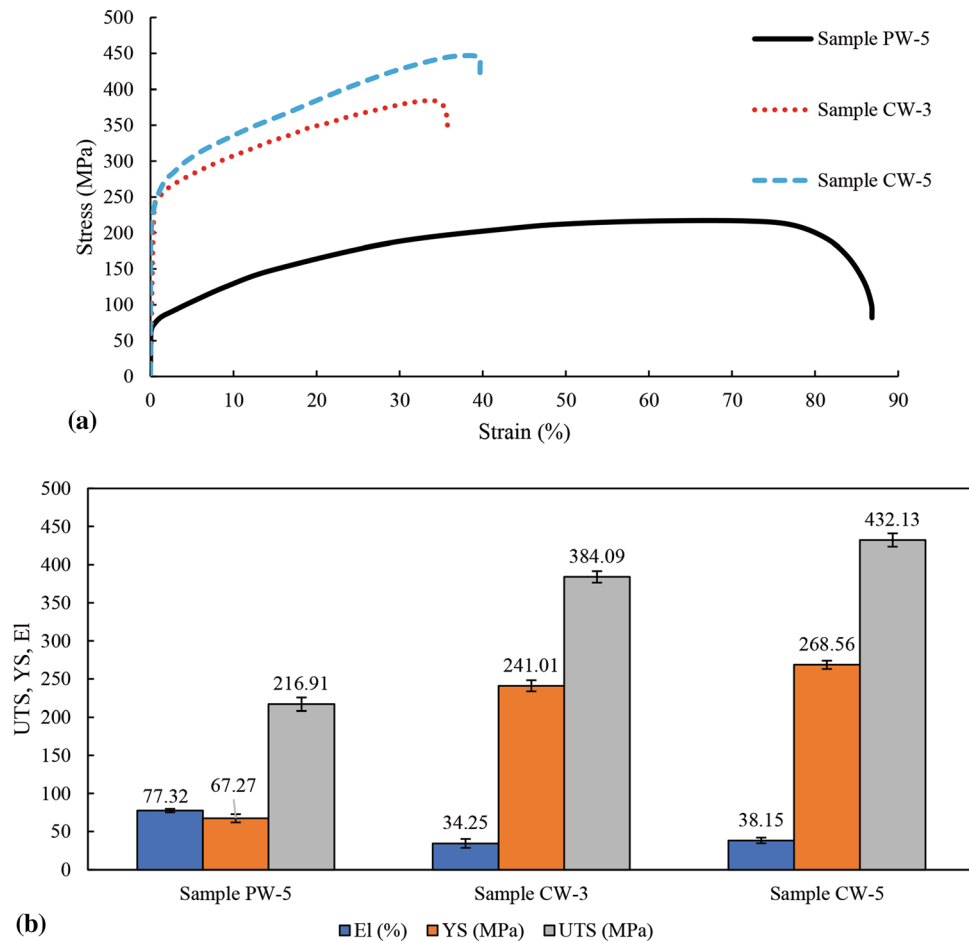


Fig. 13 (a) Strain–stress curve of different samples, (b) the ultimate tensile strength (UTS), yield strength (YS), and elongation (EI) of different samples

indicates that all extruded wires experienced huge plastic deformation before failure. Also, tear ridges are visible, demonstrating ductile deformation before failure (Ref 29, 30). Although sample PW-5 had finer grains, its dimples were as big as the sample CW-5, suggesting that sample PW-5 experienced higher plasticity according to its elongation. The fracture surfaces of samples CW-3 and CW-5 were different from each other, primarily due to their different plasticity levels. The pull-out of Ti_2SnC reinforcement in the fracture surface of sample CW-3 shows that cracks were started at the porosities between Cu and Ti_2SnC and propagated along the weak bonding. On the other hand, sample CW-5 exhibited a transgranular fracture due to good interfacial bonding.

The electrical conductivity of PW-5, CW-5, and CW-3 was 96.32 ± 1.32 , 89.21 ± 1.43 , and 84.65 ± 1.76 % IACS, respectively. The rule of mixtures was assumed to predict the electrical conductivity of Cu-5 vol.% Ti_2SnC composite. Since all composite wires had the same volume percent, the predicted electrical conductivity was 86.96 % IACS. Factors such as impurities, point defects, dislocations, grain boundaries, pores, and voids contributed to the reduction of electrical conductivity. Porosities and dislocations, in particular, acted as electron scattering sites and significantly reduced electrical conductivity. Moreover, as an impurity, Ti_2SnC particles decreased the electrical conductivity of composite wires. In sample CW-3, there were higher porosities, particularly at the interface of Cu

and Ti_2SnC phases and grain boundaries. Although sample CW-5 has a more solid solution and intermetallic formation at the interface, sample CW-3 appeared to have lower electrical conductivity due to its higher porosities and grain boundaries. However, it is important to note that proper interfacial bonding resulted in higher electrical conductivity than the predicted value.

Figure 15 illustrates the wear rate and friction coefficient of samples PW-5, CW-3, and CW-5. Wear rate is calculated as a ratio of worn mass loss to sliding distance. The wear rate of the samples PW-5, CW-3, and CW-5 was 0.99, 0.32, and 0.15×10^{-2} mg/m, respectively. The improvement in wear resistance of composite wires is because of the increment of hardness. According to Archard's equation (Ref 31), metal hardness and wear resistance have a direct relationship. Also, compared with pure copper wire, the high load bearing of Ti_2SnC particles reduced the direct contact from the abrasive disk. The large ductility and plasticity during pure copper wire wearing caused an adhesive mechanism, which resulted in increased material removal.

The friction coefficient of samples PW-5, CW-3, and CW-5 were 0.69, 0.41, and 0.31, respectively. The decrease in the friction coefficient of composite wires can be attributed to the increase in surface hardness, which results in a smaller contact area, and the Ti_2SnC particles, which act as solid lubricants. Due to its high c/a ratio (generally greater than 4), the MAX

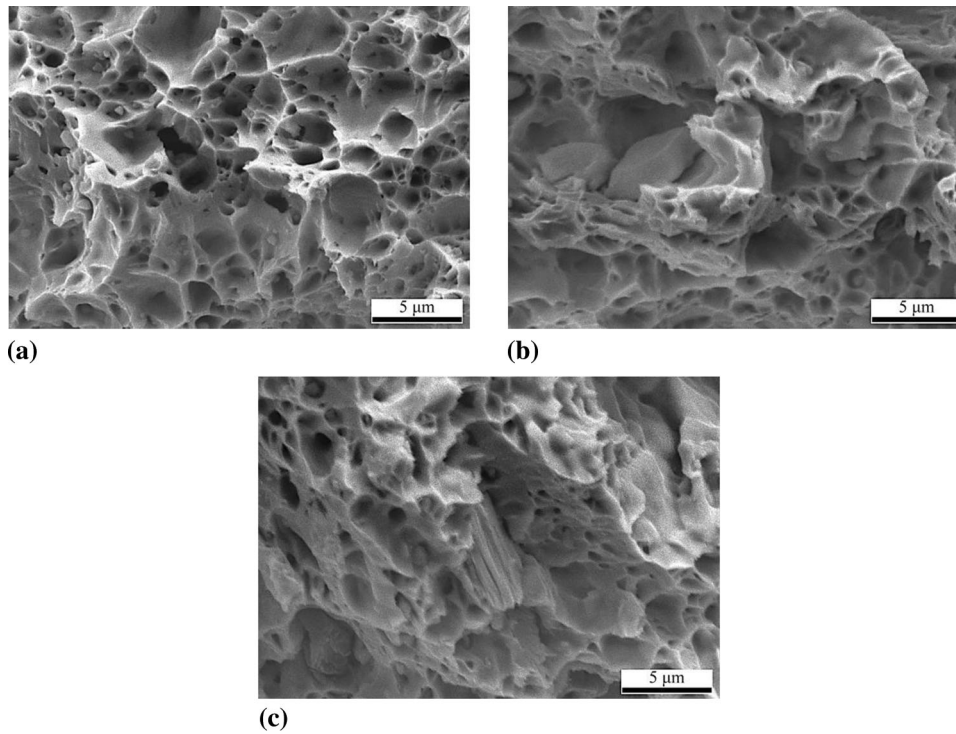


Fig. 14 SEM image of fracture surface of; (a) sample PW-5, (b) sample CW-3, (c) sample CW-5

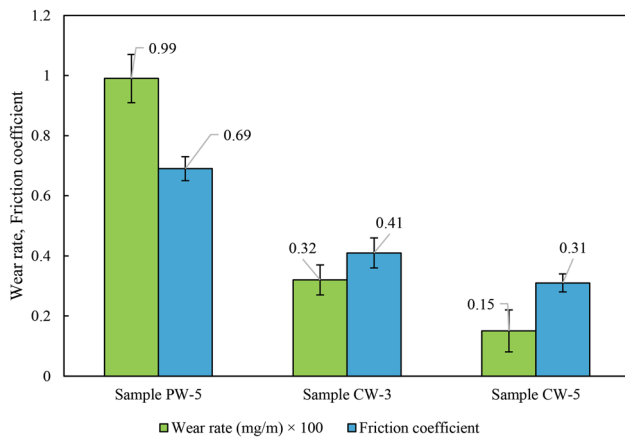


Fig. 15 The wear rate and friction coefficient of different samples

phase exhibits dramatic tribological properties. In addition, the decrement in friction coefficient indicates that composite layer removal was reduced, leading to an alternative wear mechanism to the adhesive mechanism. In sample CW-5, proper bonding at the interface of Cu and Ti_2SnC increased hardness and consequently enhanced wear resistance. More porosities at the surface, particularly at the interface of the sample CW-3, reduced the contact surface area, thus increasing the net load of wear. This resulted in lower wear resistance of sample CW-3 compared to sample CW-5.

Figure 16 shows SEM images of the worn surface of samples PW-5, CW-3, and CW-5. Due to contact of the pin and abrasive disk in some regions, the plastic deformation sites are formed, which causes to increase in the friction coefficient. Work-hardening sites resisted mass loss associated with the adhesive wear mechanism. On the other hand, they led to the

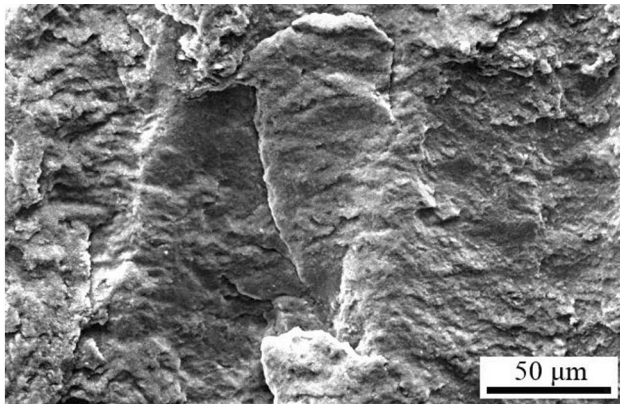
formation of microcracks and cavities. According to Fig. 16(a), as microscopic cracks grew, the surface layer was removed, thereby producing a delamination wear mechanism. However, due to the presence of Ti_2SnC particles, severe plastic deformation was prevented, and the wear rate was reduced (Fig. 16b, c).

A poor interfacial bond between Cu and Ti_2SnC caused more ploughing of reinforcement in sample CW-3 and led to severe abrasive wear. Moreover, the detachment mechanism was present in both composite wires, indicating a delamination mechanism. Nevertheless, peeling pits on the surface of sample CW-5 were significantly lower than those on sample CW-3, suggesting the formation of a milder delamination mechanism. Once again, this can be attributed to poor interfacial bonding that facilitates crack formation and propagation, creating a severe delamination wear mechanism. The smoother surface in some regions of sample CW-5 is indicative of an oxidative wear mechanism. The wear mechanism was observed at low load levels after a low abrasive wear rate. (The load in this study was 20N, which is very low.) Consequently, the formed oxides lubricated the surface and reduced wear, resulting in the transition to oxidative wear instead of abrasive wear (Ref 32).

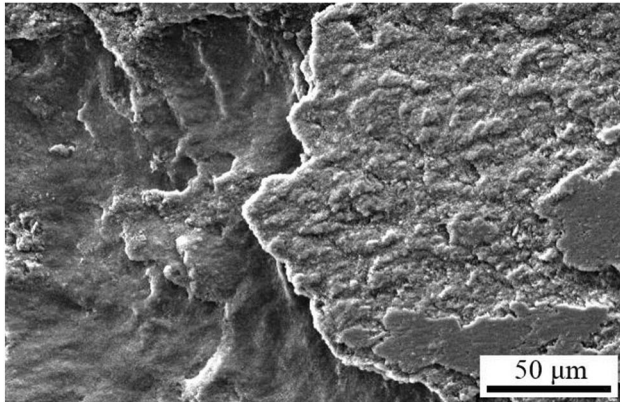
5. Conclusion

This study investigated the effect of FSBE-processed Cu-5 vol.% Ti_2SnC composite wire with 3 and 5 mm diameters on microstructure, mechanical properties, electrical conductivity, and wear resistance. Here are some of the main results:

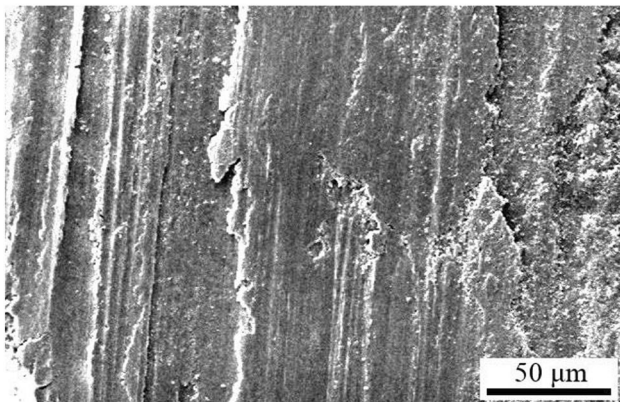
- The grain size of both composite wires with 3 and 5 mm diameters was higher than the primary composite. By decreasing the composite wire diameter from 5 to 3 mm,



(a)



(b)



(c)

Fig. 16 SEM image of wear surface of; (a) sample PW-5, (b) sample CW-3, (c) sample CW-5

the grain size decreased from 8.5 ± 0.5 to $6.3 \pm 0.7 \mu\text{m}$.

- By increasing the composite wire diameter from 3 to 5 mm, the porosity in the copper matrix was reduced, and the quality of the Cu-Ti₂SnC interface was enhanced.
- By increasing composite wire diameter, due to a higher temperature and plastic deformation during FSBE, a higher amount of Cu (Sn) solid solution and Cu₈₁Sn₂₂ intermetallic was formed in the microstructure.
- By increasing composite wire diameter from 3 to 5 mm, the ultimate tensile strength, hardness, and wear resistance increased by 13, 10, and 53 %, respectively.
- The composite wire with 3 and 5 mm diameters exhibited electrical conductivity of 84.65 ± 1.76 and

$89.21 \pm 1.43\%$ IACS, respectively. The electrical conductivity and wear resistance of Cu-5 vol.% Ti₂SnC composite wire with a diameter of 5 mm were 7% lower and 85% higher, respectively, than FSBE-processed pure copper wire with a similar diameter.

References

1. B. Yokesh Kumar and P. Sevel, Impact of Traverse Speed during Joining of CDA101 Plates Using FSW Process, *Sci. Iran.*, 2022, **29**, p 1817–1827
2. W. Yu, J. Guérolé, J. Ghanbaja, M. Vallet, and A. Guitton, Frank Partial Dislocation in Ti₂AlC-MAX Phase Induced by Matrix-Cu Diffusion, *Scr. Mater.*, 2021, **191**, p 34–39
3. X. Huang, Y. Feng, G. Qian, H. Zhao, J. Zhang, and X. Zhang, Physical, Mechanical, and Ablation Properties of Cu-Ti₃AlC₂ Composites with Various Ti₃AlC₂ Contents, *Mater. Sci. Technol.*, 2018, **34**, p 757–762
4. W. Hu, Z. Huang, Y. Wang, X. Li, H. Zhai, Y. Zhou, and L. Chen, Layered Ternary MAX Phases and Their MX Particulate Derivative Reinforced Metal Matrix Composite: A Review, *J. Alloys Compd.*, 2021, **856**, p 157313
5. A. Jamwal, P. Mittal, R. Agrawal, S. Gupta, D. Kumar, K.K. Sadasivuni, and P. Gupta, Towards Sustainable Copper Matrix Composites: Manufacturing Routes with Structural, Mechanical, Electrical and Corrosion Behaviour, *J. Compos. Mater.*, 2020, **54**, p 2635–2649
6. M. Khaloobagheri, B. Janipour, N. Askari, and E. Shafiee Kamal Abad, Characterisation of Powder Metallurgy Cu-ZrO₂ Composites, *Adv. Prod. Eng. Manag.*, 2013, **8**, p 242–248
7. X. Ma, E. Nickerson, T. Wang, D. Zhang, T. Pelletiers, S. Whalen, and X. Li, Friction Extrusion of ODS Copper Rod Made from Powder, *J. Manuf. Process.*, 2022, **84**, p 223–229
8. M. Akbari and P. Asadi, Optimization of Microstructural and Mechanical Properties of Brass Wire Produced by Friction Stir Extrusion Using Taguchi Method, *Proc. Inst. Mech. Eng. Part L J. Mater. Des. Appl.*, 2021, **235**, p 2709–2719
9. M.A. Ansari, R.A. Behnagh, M. Narvan, E.S. Naeini, M.K.B. Givi, and H. Ding, Optimization of Friction Stir Extrusion (FSE) Parameters through Taguchi Technique, *Trans. Indian Inst. Met.*, 2016, **69**, p 1351–1357
10. D. Baffari, G. Buffa, and L. Fratini, Influence of Process Parameters on the Product Integrity in Friction Stir Extrusion of Magnesium Alloys, *Key Eng. Mater.*, 2016, **716**, p 39–48
11. D. Baffari, G. Buffa, D. Campanella, and L. Fratini, Al-SiC Metal Matrix Composite Production through Friction Stir Extrusion of Aluminum Chips, *Procedia Eng.*, 2017, **207**, p 419–424
12. C. Satheesh, P. Sevel, and R.S. Kumar, Experimental Identification of Optimized Process Parameters for FSW of AZ91C Mg Alloy Using Quadratic Regression Models, *Stroj. Vestn. J. Mech. Eng.*, 2020, **66**, p 736
13. P. Sevel, C. Satheesh, and R.S. Kumar, Generation of Regression Models and Multi-response Optimization of Friction Stir Welding Technique Parameters during the Fabrication of AZ80A Mg Alloy Joints, *Trans. Can. Soc. Mech. Eng.*, 2019, **44**, p 311–324
14. A. Jahani, H.J. Aval, M. Rajabi, and R. Jamaati, Effects of Ti₂SnC MAX Phase on Microstructure, Mechanical, Electrical, and Wear Properties of Stir-Extruded Copper Matrix Composite, *Adv. Eng. Mater.*, 2023, **25**, p 2201463
15. R.A. Behnagh, N. Shen, M.A. Ansari, M. Narvan, M.K.B. Givi, and H. Ding, Experimental Analysis and Microstructure Modeling of Friction Stir Extrusion of Magnesium Chips, *J. Manuf. Sci. Eng.*, 2016 <https://doi.org/10.1115/1.4031281>
16. A. Heidarzadeh, S. Mironov, R. Kaibyshev, G. Çam, A. Simar, A. Gerlich, F. Khodabakhshi, A. Mostafaei, D.P. Field, and J.D. Robson, Friction Stir Welding/Processing of Metals and Alloys: A Comprehensive Review on Microstructural Evolution, *Prog. Mater. Sci.*, 2021, **117**, p 100752

17. P. Asadi and M. Akbari, Numerical Modeling and Experimental Investigation of Brass Wire Forming by Friction Stir Back Extrusion, *Int. J. Adv. Manuf. Technol.*, 2021, **116**, p 3231–3245
18. M. Dickson, The Significance of Texture Parameters in Phase Analysis by X-ray Diffraction, *J. Appl. Crystallogr.*, 1969, **2**, p 176–180
19. C. Salvo, E. Chicardi, J. Hernández-Saz, C. Aguilar, P. Gnanaprakasam, and R. Mangalaraja, Microstructure, Electrical and Mechanical Properties of Ti₂AlN MAX Phase Reinforced Copper Matrix Composites Processed by Hot Pressing, *Mater. Charact.*, 2021, **171**, p 110812
20. M. Barmouz and M.K.B. Givi, Fabrication of In Situ Cu/SiC Composites Using Multi-pass Friction Stir Processing: Evaluation of Microstructural, Porosity, Mechanical and Electrical Behavior, *Compos. Part A Appl. Sci. Manuf.*, 2011, **42**, p 1445–1453
21. R.A. Behnagh, A. Samanta, M.A.M. Pour, P. Esmailzadeh, and H. Ding, Predicting Microstructure Evolution for Friction Stir Extrusion Using a Cellular Automaton Method, *Model. Simul. Mater. Sci. Eng.*, 2019, **27**, p 035006
22. H. Zhang, X. Li, X. Deng, A.P. Reynolds, and M.A. Sutton, Numerical Simulation of Friction Extrusion Process, *J. Mater. Process. Technol.*, 2018, **253**, p 17–26
23. T.R. Jaramillo, “Modeling and Optimization of a Friction Stir Extrusion Process Using Finite Element Methods,” Master’s Thesis, University of Notre Dame, 2018. <https://doi.org/10.7274/mk61rf58z66>
24. J. Wu, Y. Zhou, J. Wang, W. Wang, and C. Yan, Interfacial Reaction between Cu and Ti₂SnC during Processing of Cu-Ti₂SnC Composite, *Int. J. Mater. Res.*, 2022, **96**, p 1314–1320
25. A. Bahador, J. Umeda, E. Hamzah, F. Yusof, X. Li, and K. Kondoh, Synergistic Strengthening Mechanisms of Copper Matrix Composites with TiO₂ Nanoparticles, *Mater. Sci. Eng. A*, 2020, **772**, p 138797
26. C. Wang, H. Lin, Z. Zhang, and W. Li, Fabrication, Interfacial Characteristics and Strengthening Mechanisms of ZrB₂ Microparticles Reinforced Cu Composites Prepared by Hot-Pressed Sintering, *J. Alloys Compd.*, 2018, **748**, p 546–552
27. F. Long, X. Guo, K. Song, S. Jia, V. Yakubov, S. Li, Y. Yang, and S. Liang, Synergistic Strengthening Effect of Carbon Nanotubes (CNTs) and Titanium Diboride (TiB₂) Microparticles on Mechanical Properties of Copper Matrix Composites, *J. Mater. Res. Technol.*, 2020, **9**, p 7989–8000
28. M. Barmouz, P. Asadi, M.B. Givi, and M. Taherishargh, Investigation of Mechanical Properties of Cu/SiC Composite Fabricated by FSP: Effect of SiC Particles’ Size and Volume Fraction, *Mater. Sci. Eng. A*, 2011, **528**, p 1740–1749
29. X. Chen, J. Tao, J. Yi, Y. Liu, C. Li, and R. Bao, Strengthening Behavior of Carbon Nanotube-Graphene Hybrids in Copper Matrix Composites, *Mater. Sci. Eng. A*, 2018, **718**, p 427–436
30. J. Zhang and Y. Zhou, Microstructure, Mechanical, and Electrical Properties of Cu-Ti₃AlC₂ and In Situ Cu-TiC_x Composites, *J. Mater. Res.*, 2008, **23**, p 924–932
31. J. Archard, Contact and Rubbing of Flat Surfaces, *J. Appl. Phys.*, 1953, **24**, p 981–988
32. Y. Zhan and G. Zhang, Friction and Wear Behavior of Copper Matrix Composites Reinforced with SiC and Graphite Particles, *Tribol. Lett.*, 2004, **17**, p 91–98

Publisher’s Note Springer Nature remains neutral with regard to jurisdictional claims in published maps and institutional affiliations.

Springer Nature or its licensor (e.g. a society or other partner) holds exclusive rights to this article under a publishing agreement with the author(s) or other rightsholder(s); author self-archiving of the accepted manuscript version of this article is solely governed by the terms of such publishing agreement and applicable law.